Electronic Supplementary Material (ESI) for ChemComm.
This journal is © The Royal Society of Chemistry 2023

Supplementary Information

Ion-Selective Response of Visible Light Photoswitchable Indole-hemithioindigo: Toward Chemical Sensing of Fluoride and Hydroxide

Weian Zhang,[a] Yi Lu,[b] Yu Cheng,[b] Yifu Wang,[b] Zeying Wu,[c] Jingying Zhai,[b] and Xiaojiang Xie*[b]

Email: xiexj@sustech.edu.cn

[a] School of Chemistry and Chemical Engineering, Harbin Institute of Technology, Harbin 150001, China

[b] Department of Chemistry, Southern University of Science and Technology, Shenzhen 518055, China

[c] School of Chemical Engineering and Material Science, Changzhou Institute of Technology, Changzhou 213032, China

Table of Contents

1. Experimental section

1.1 Materials and reagents

Benzo[b]thiophen-3(2H)-one and 1H-indole-2-carbaldehyde were purchased from Bide Pharmatech Ltd. Acetonitrile (CH_3CN), ethanol (EtOH) and dimethyl sulfoxide (DMSO), tetrahydrofuran (THF), N,N-dimethylformamide (DMF), methanol(CH_3OH) and chloroform-d ($CDCl_3$) were purchased from J&K Scientific Ltd. in China. Ethyl acetate (EA), dichloromethane (CH_2Cl_2), and dimethyl sulfoxide-d_6 (DMSO-d_6) were purchased from Energy Chemical. Methanol-d_4 (CD_3OD) was purchased from CIL. Toluene(C_7H_8) and ethyl ether absolute ($C_4H_{10}O$) were purchased from Shanghai Lingfeng Chemical Reagent Co. Sodium chloride, potassium chloride, magnesium chloride, calcium chloride, iron(II)chloride tetrahydrate, iron(III) chloride hexahydrate, copper(II) chloride, zinc chloride, lead nitrate, aluminum chloride, sodium nitrate, sodium sulfocyanate, sodium sulfate, sodium perchlorate, sodium iodide, sodium bromide, sodium Fluoride, sodium dihydrogen phosphate, and tetradodecylammonium chloride (TDDA) were of analytical grade and obtained from Sigma-Aldrich. Poly(ethylene terephthalate) (PET) support was obtained from Huiying Plastic Material Factory. Polyurethane hydrogel (HydroMed D640) was obtained from AdvanSource biomaterials. pH buffers were prepared from a 0.02 M phosphate buffer solution (PBS, pH=3.0, 4.0, 5.0, 6.0, 7.0, 8.0) containing sodium dihydrogen phosphate, and adjusted to a desired pH with 1 M HCl or NaOH solution. Deionized water was used after purification by Milli-Q Integral 5.

1.2 Instrumentation

Ultraviolet-visible (UV-vis) absorption spectra were obtained with Thermo Fisher Scientific (Evolution 220). To measure the absorption spectra of HTI-In under external light irradiation, a quartz cuvette (3 mm light path, Hellma, Germany) was used with illumination from an external LED light source (LED4D232, Thorlabs). Fluorescence spectra were measured on a fluorescence spectrometer (Fluorolog-3, Horiba Jobin Yvon) with excitations at 455 nm. HTI-In (50 μg/mL) was dissolved in methanol and characterized by a Q-Exactive electrospray ionization mass spectrometer (ESI-MS) in the positive-ion mode (Thermo Fisher Scientific, USA). The ^{1}H-NMR and ^{13}C-NMR spectra of HTI-In in 600 μL of DMSO-d_6 /CD_3OD/CDCl3 before and after light irradiation were measured by Brüker AVANCE NEO 400 (^{1}H: 400 MHz, ^{13}C: 101 MHz) and Brüker AVANCE NEO 600 (^{1}H: 600 MHz, ^{13}C: 150 MHz). Chemical shifts (δ) are given relative to tetramethylsilane as external standard. For ^{1}H NMR: $CDCl_3$ = 7.26 ppm, DMSO-d_6 = 2.50 ppm, CD_3OD = 3.31 ppm. For ^{13}C NMR: DMSO-d_6 = 39.52 ppm. The resonance multiplicity is indicated as s = singlet, d = doublet, t = triplet, q = quartet, m = multiplet and br = broad signal. The chemical shifts are given in parts per million (ppm) on the delta scale (δ), and the coupling constant values (J) are in hertz (Hz). Infrared spectra were recorded on a BOEN-85697 (Fairborn). X-ray photoelectron spectroscopy (XPS) was measured via a PHI 5000 VersaProbe III instrument(ULVAC) with Al Kα irradiation. Samples for XPS were prepared by drying the HTI-In powder using a vacuum freeze dryer (CHRIST, Alpha 1-2 LDplus). The binding energy was calibrated with C 1s signal (284.8 eV) as the reference.

1.3 Synthesis of HTI-In

HTI-In was prepared according to the general procedure using Benzo[b]thiophen-3 (2H)-one (83 mg, 0.5 mmol), 1H-indole-2-carbaldehyde (73 mg, 0.5 mmol), EtOH (10 mL) and piperidine (1 drop). The reaction mixture was stirred for overnight at 80 °C. The crude product was purified by column

chromatography (SiO_2, CH_2Cl_2/CH_3OH 100:1). Obtained as a red solid (110.3 mg, 77.5%). ^{1}H NMR (DMSO-d_6, 400 MHz): δ 7.96 (s, 1H), 7.87 (d, J = 7.7 Hz, 1H), 7.82 (d, J = 7.9 Hz, 1H), 7.77 – 7.69 (m, 2H), 7.49 – 7.39 (m, 2H), 7.25 (dd, J = 8.2, 7.0 Hz, 1H), 7.12 – 7.06 (m, 2H). ^{13}C-NMR (DMSO-d_6, 101 MHz): δ 186.28, 145.41, 137.77, 135.57, 134.34, 132.09, 129.51, 127.92, 127.43, 126.74, 126.01, 125.55, 124.30, 121.76, 120.72, 113.75, 112.84. ESI-MS (m/z): $[M+H]^+$ calc'd for $C_{17}H_{12}NOS^+$: 278.0634, found 278.0630.

1.4 UV-Vis spectroscopic measurements of HTI-In

Ultraviolet-visible (UV-Vis) absorption spectra were recorded in a quartz cuvette (3 mm light path, Hellma, Germany) for organic solutions and an external multiwavelength LED source (455 nm, 530 nm, 625 nm) was used to irradiate the solutions. Experimentally, all solutions were illuminated by an optical fiber on top of the sample solutions at controlled distance and intensity. To determine the photostationary states (PSS), different illumination time was investigated and the absorption spectra were monitored over time. Unless otherwise specified, all solutions in the cuvette were 60 μL and were tested at 25 ℃ in the dark. The wavelength for the kinetic monitoring of the absorbance of the solutions was according to the peak maxima of absorption spectra. Temperature was controlled at 25 ℃ or as indicated with the water-cooled Peltier accessories.

1.5 Fluorescence spectrophotometry of HTI-In

Steady-state fluorescence spectroscopy was performed with a quartz cuvette (3 mm light path, Hellma, Germany). Light with different wavelengths was introduced through an optical fiber on top of the sample solutions. Unless stated differently, all tests were performed at a default concentration of 400 μM.

1.6 Preparation of sensor films

Typically, 0.5 mg HTI-In, 0.36 mg TDDA were dissolved in a hydrogel HydroMed D640 stock solution (1 mL 10 wt% in EtOH/H_2O). The "cocktail" was coated onto a dust-free PET substrate using the classical knife-coating method under 617 nm light to prepare hydrogel films with 20 μm thickness. The hydrogel films were stored in dark and rinsed with deionized water before use.

2. Photoisomerization under continuous irradiation

2.0 mM solutions of HTI-In in different solvents (600 μL) were prepared in NMR tubes. Firstly, a ^{1}H NMR spectrum was recorded before illumination with 455 nm LED to determine if the samples contained already *E* isomer. The sample was illuminated with 455 nm LED for *Z*/*E* photoisomerization and then another ^{1}H NMR spectrum was measured. The new NMR signals of the *E* isomer were integrated and compared to the signals of remaining *Z* isomer to calculate the percentage of *E* isomer after illumination. In order to obtain the total E isomer composition at the photostationary state (PSS), illumination was continued until no obvious change in the composition between the two isomers(*Z*/*E*) was observed. In Table S1 the isomer yields in the PSS are given.

Table S1. Isomer yields obtained in the PSS after *Z* to *E* photoisomerization of 2 mM solutions of the respective HTI-In in different solvents. The wavelengths used and duration times of the irradiation are given in brackets.

HTI	Solvent	*% E* isomer
HTI-In	$CDCl_3$	89% (20 min, 455 nm)
	CD_3OD	60% (40 min, 455 nm)
	DMSO-d_6	90% (30 min, 455 nm)

3. Photoisomerization quantum yields

The photoisomerization quantum yield was determined using the measuring method as described by Henry Dube and has been modified to some extent.[1] The photoisomerization quantum yield of HTI-In was measured by irradiation at a suitable wavelength (455 nm) while monitoring the absorbance change of the sample. The change in the absorption was fit with mono-exponential decay ($y=A_1*\exp(-x/t_1)+y_0$) to retrieve the apparent rate constant k ($k=1/t_1$). By changing the light intensity of appropriate wavelength, the linear relationship between k and light intensity (I) can be obtained and the slope was recorded as m. The quantum yield can be calculated by equation (*S1*)

$$\phi_{Z/E} = \frac{h \cdot c \cdot N_A \cdot S}{\lambda_{ex} \cdot P \cdot \varepsilon} \cdot m \qquad (S1)$$

The meanings of each letter in the formula are as follows: *h* = Planck´s constant (6.626×10^{-34} Js), *c* = speed of light (2.9979×10^{8} ms^{-1}), N_A = Avogadro constant, S = effective light area, P = power of the laser, λ_{ex} = excitation wavelength, ε = extinction coefficient at the appropriate wavelength, *m* = slope. The calculated quantum yields are given in Table S2.

Table S2. Photoisomerization quantum yields ($\phi_{Z/E}$) of HTI-In in different solvents.

HTI	Solvent	λ_{ex} / nm	P / mW	λ_{probe} / nm	$\phi_{Z/E}$ / %
HTI-In	toluene	455	0.3-20	519	48.18±1.47
	THF	455	0.3-20	517	33.69±0.96
	CH_3OH	455	0.3-20	512	26.38±1.05
	DMSO	455	0.3-20	515	43.90±1.02

4. Supplementary figures

^{1}H NMR spectra of (*Z*)-HTI-In:

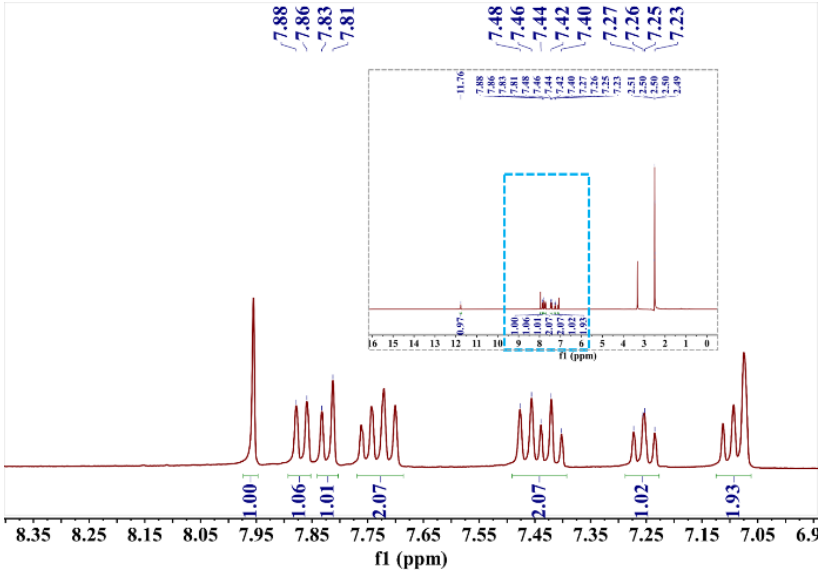

^{1}H NMR spectra of (*E*)-HTI-In:

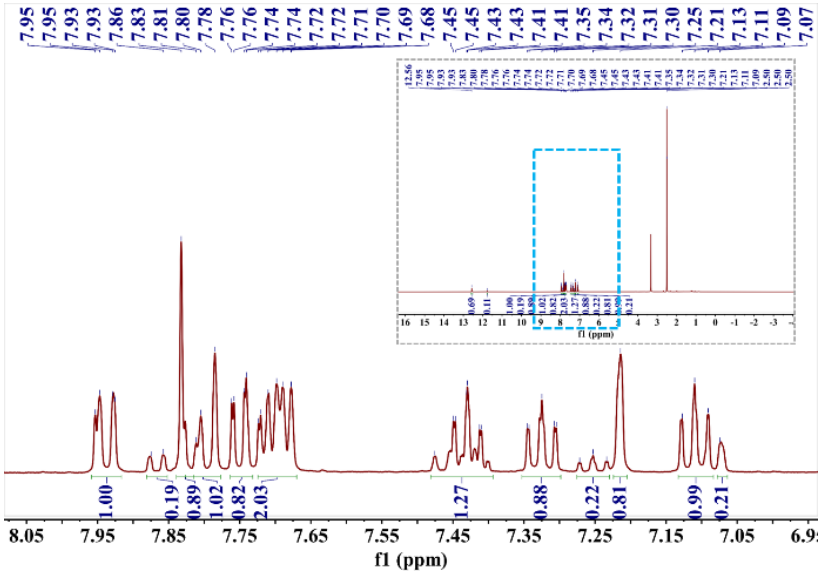

Note: the percentage of *E* isomer (90%) was calculated.

^{13}C NMR spectra of HTI-In:

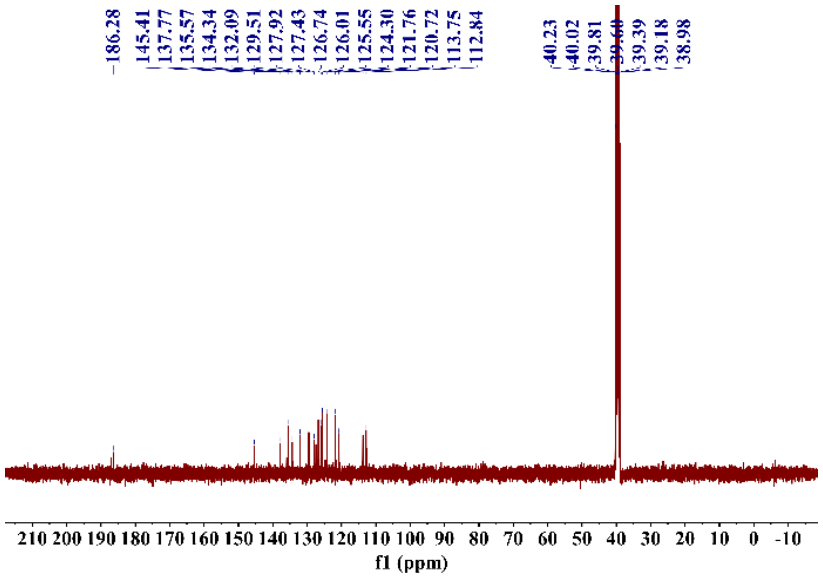

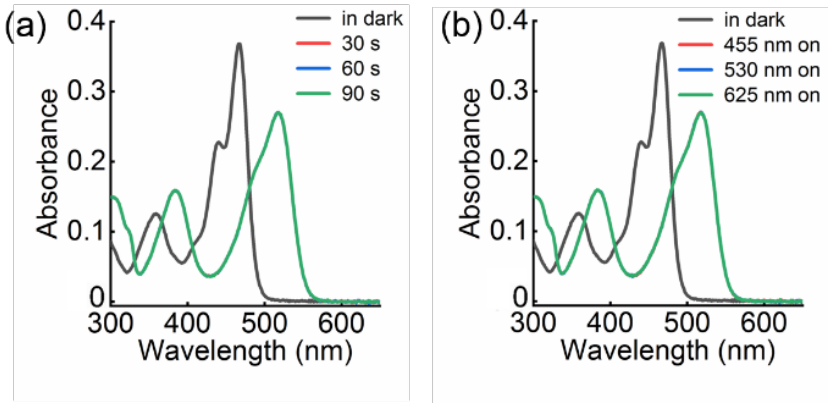

Fig. S1. (a) UV-Vis absorption spectra of HTI-In (40 μM in toluene) in the dark (black line) and upon reaching the photostationary state (red to green line) after irradiation at 455 nm (7.06 mW/cm^2). (b) UV-Vis absorption spectra of HTI-In (40 μM in toluene) in the dark (black) and upon reaching the photostationary state (red) after irradiation at 455 nm (7.06 mW/cm^2, 0.5 min), then consecutively irradiated with light at 530 nm (3.54 mW/cm^2, 0.5 min) and 625 nm (3.28 mW/cm^2, 0.5 min), respectively. The red, blue, and green traces in the figure are completely overlapped.

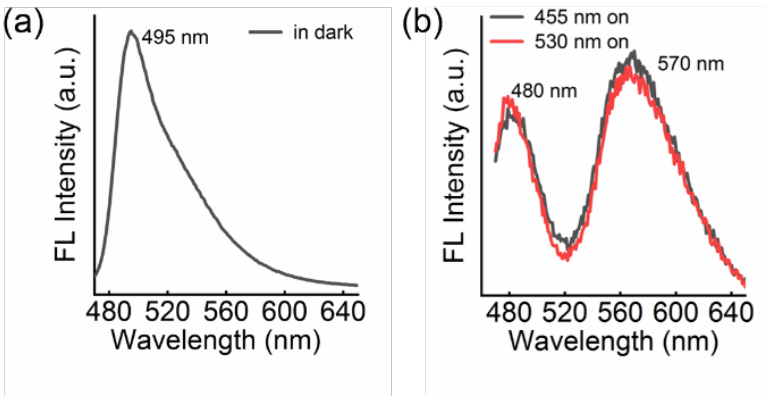

Fig. S2. (a) Fluorescence emission spectra of HTI-In (20 μM) in toluene solution before illumination with 455 nm light. (b) Fluorescence emission spectra of HTI-In (20 μM) in toluene solution after consecutively irradiated with light at 455 nm (7.06 mW/cm^2, 0.5 min) and 530 nm (3.54 mW/cm^2, 0.5 min), respectively.

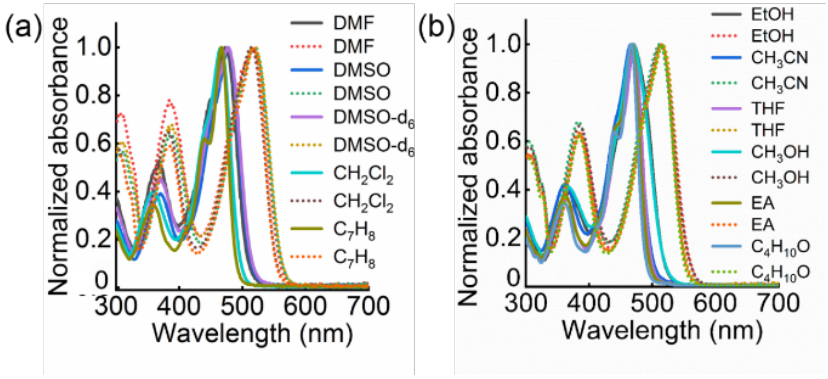

Fig. S3. (a-b) UV-Vis absorption spectra of HTI-In (80 μM) in the dark (solid line) and after saturating illumination with 455 nm (91.32 mW/cm^2, 10 min, dashed line) in common organic solvents in the laboratory. Normalized by the maximum absorbance values.

Table S3. Quantification of isomer band separation of HTI-In with respect to solvents

Solvent	DMSO	DMSO-d_6	CH_3CN	CH_3OH	THF	EA
Band separation(nm)	43	43	45	45	46	46
Solvent	DMF	EtOH	$C_4H_{10}O$	CH_2Cl_2	C_7H_8	
Band separation(nm)	46	47	48	51	52	

By measuring the absorbance spectra of HTI-In molecules before and after illumination with 455 nm LED in different solvents, we found that the band separation between the isomers' absorption maxima decrease with the ability of solvent to form hydrogen bond.

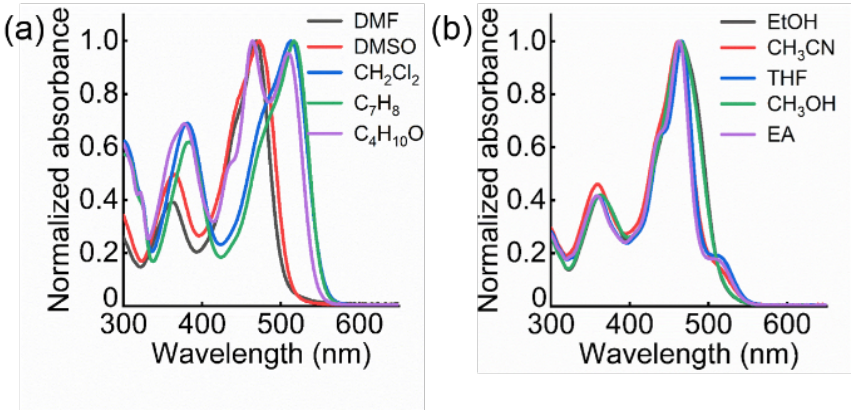

Fig. S4. (a,b) UV-Vis absorption spectra of HTI-In (80 μM) after saturating illumination with 455 nm ((91.32 mW/cm^2, 10 min, dashed line) in common organic solvents in the laboratory and then left

in the dark for one month . Absorption values are normalized.

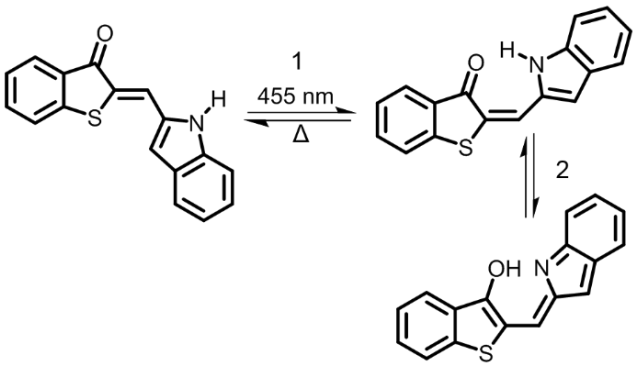

Scheme S1. A schematic illustration of HTI-In undergoing visible light responsive double bond isomerization (procedure 1) and a keto-enol tautomerization occurring in the *E*-configuration of HTI-In (procedure 2).

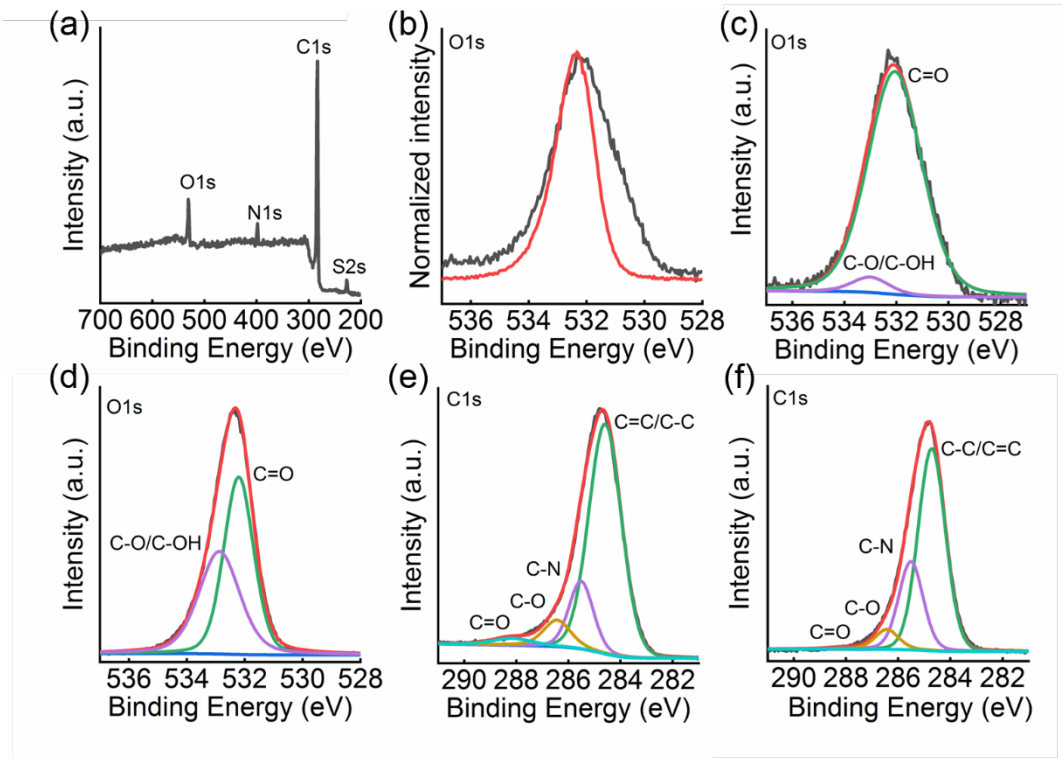

Fig. S5. (a) The wide spectra of HTI-In. (b) O 1s spectra of HTI-In before (black) and after (red) illuminating with 455 nm (91.32 mW/cm^2, 30 min). O 1s spectra and C 1s spectra of HTI-In before (c, e) and after (d, f) illuminating with 455 nm (91.32 mW/cm^2, 30 min).

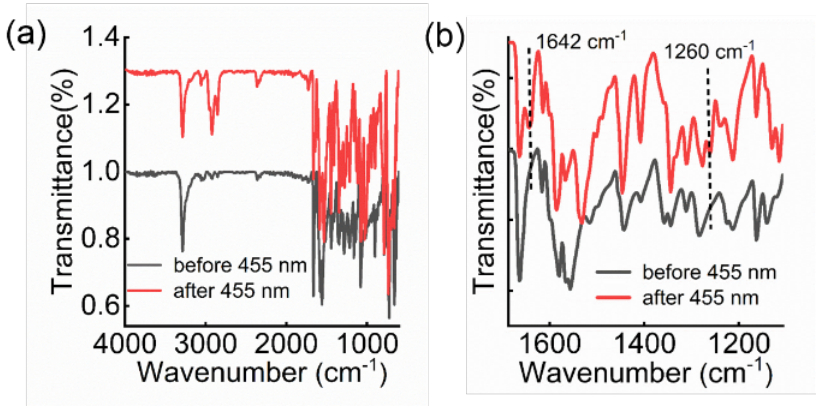

Fig. S6. (a,b) The IR spectra of HTI-In before and after illuminating with 455 nm (91.32 mW/cm^2, 30 min).

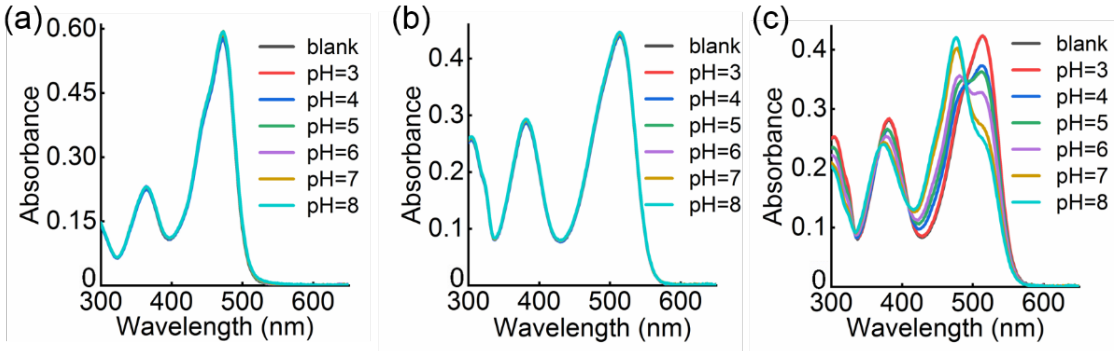

Fig. S7. UV-Vis absorption spectra of HTI-In (80 μM) in DMSO-H_2O solution (v/v=100/1) at different pOH from 11.0 to 6.0 in the dark (a) and after illumination with 455 nm light (b) (7.06 mW/cm^2, 0.5 min), then left in the dark for 8 minutes (c).

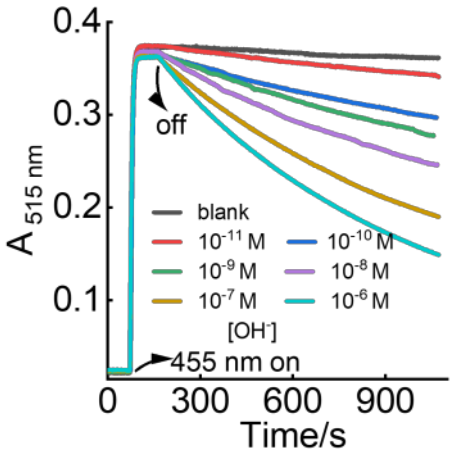

Fig. S8. Kinetic monitoring of the absorbance at 515 nm of HTI-In (80 μM) in DMSO-H_2O solution (v/v=100/1) at different OH^- concentration from 10^{-11} M to 10^{-6} M. Light irradiation at 455 nm (7.06 mW/cm^2) was switched on and off as indicated by the arrows.

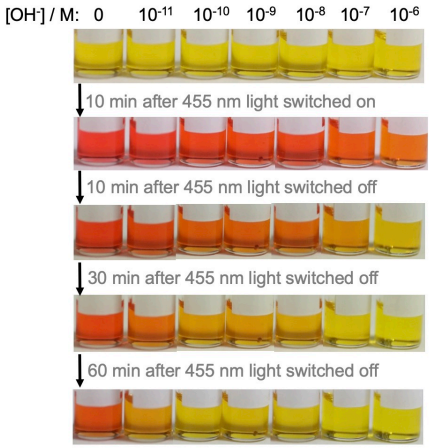

Fig. S9. Photographs showing the color changes of HTI-In (0.4 mmol) in DMSO-H_2O solution (v/v=100/1) at different hydroxide concentrations.

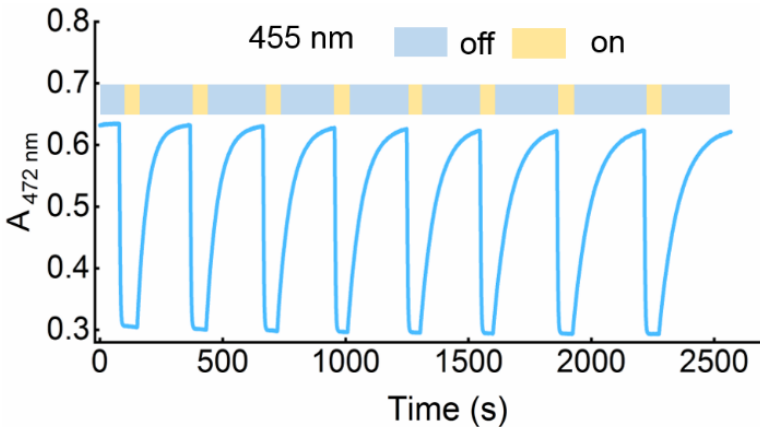

Fig. S10. Multicycle switching of HTI-In (80 μM) in DMSO-H_2O solution (v/v=100/1) upon alternating on/off of 455 nm light (7.06 mW/cm^2) at 40 degrees Celsius. [OH^-]: 10^{-6} M.

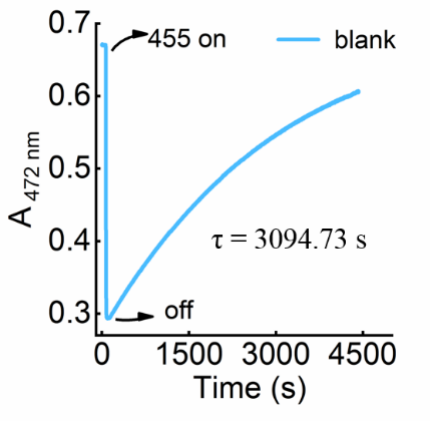

Fig. S11. Thermal relaxation of HTI-In at 40 degrees Celsius. HTI-In (80 μM, DMSO) was photoswitched from *Z* to *E* photostationary state (PSS) at 455 nm (7.06 mW/cm^2), Then turned off

the 455 nm light to allow thermal *E/Z* relaxation. [OH^-]: 10^{-11} M

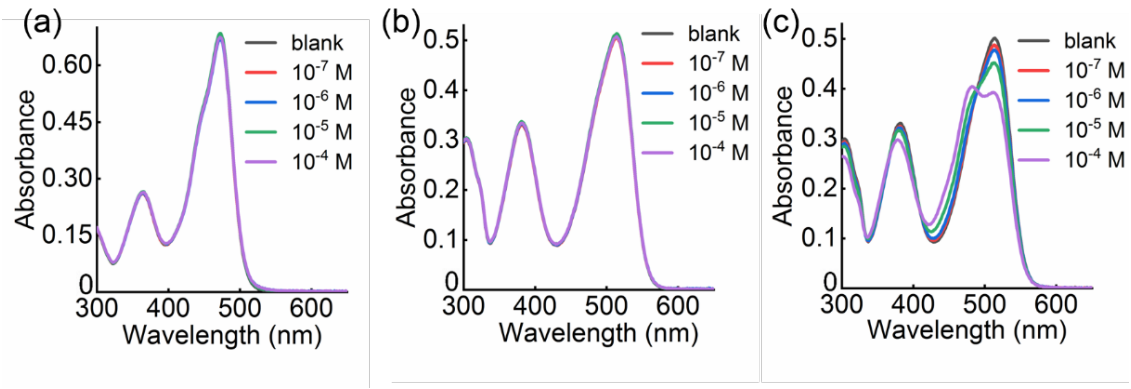

Fig. S12. UV-Vis absorption spectra of HTI-In (80 μM) in DMSO-H_2O solution (v/v=100/1) with different F^- concentrations at pH 3.0 in the dark (a), after illumination with 455 nm light (b) (7.06 mW/cm^2, 0.5 min) and then left in the dark for 4 minutes (c).

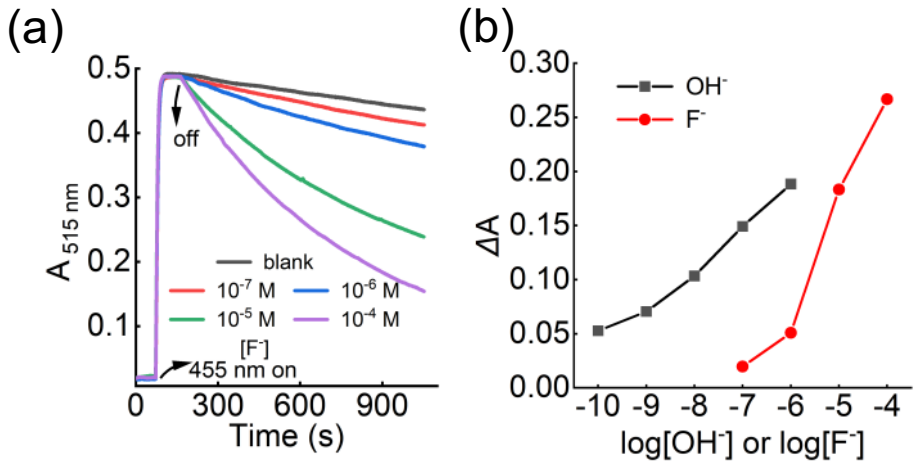

Fig. S13. (a) Kinetic monitoring of the absorbance at 515 nm of HTI-In (80 μM) in DMSO-H_2O solution (v/v=100/1) with different F^- concentrations and a fixed [OH^-] of 10^{-11} M. Light irradiation at 455 nm (7.06 mW/cm^2) was switched on and off as indicated by the arrows. (b) OH^- or F^- response calibration curves of the HTI-In based on ΔA (ΔA= $(A_{160\ s} - A_{960\ s})_{OH^-\ or\ F^-} - (A_{160\ s} - A_{960\ s})_{blank}$).

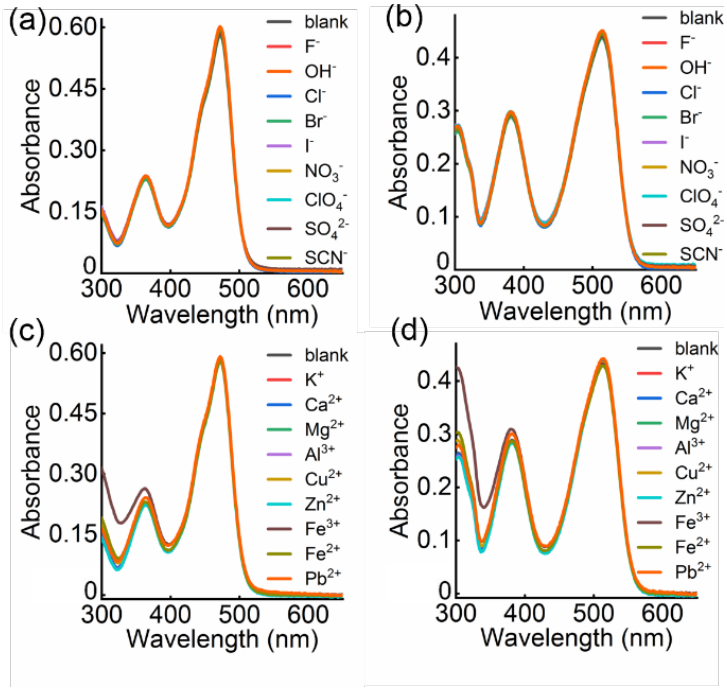

Fig. S14. UV-Vis absorption spectra of HTI-In (80 μM) in a DMSO-H_2O solution (v/v=100/1) in the presence of different anions and cations at pH 3.0 in the dark (a, c) and after illumination with 455 nm light (b, d) (7.06 mW/cm^2, 0.5 min). Hydroxide: 10^{-6} M; Other ions: 10^{-4} M.

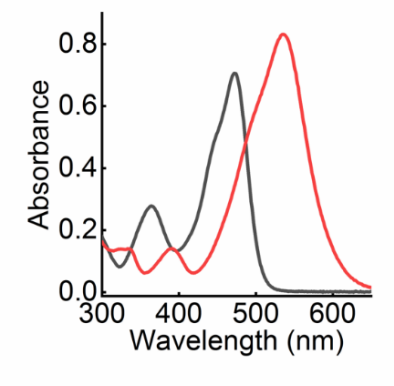

Fig. S15. UV-Vis absorption spectra of the protonated (black line) and deprotonated states (red line) of HTI-In (80 μM) in a DMSO-H_2O solution (v/v=100/1, 1 M NaOH)

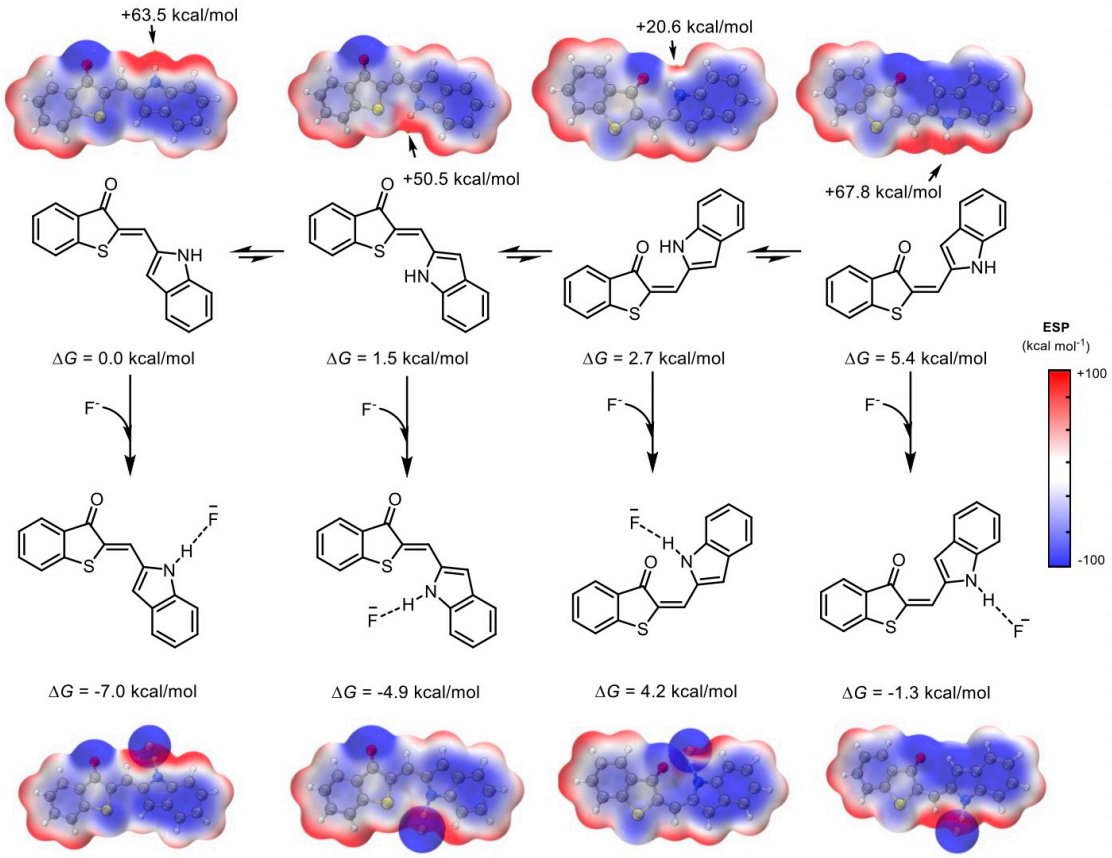

Fig. S16. Surface electrostatic potential maps of HTI-In molecule before and after the addition of fluoride ions. All computational results were performed at the M06-2X/def2-TZPV/SMD//M06-2X/6-31G(d)/SMD level of theory. Geometrical optimization and single-point energies were obtained using the Gaussian 16C.01 package, while Multiwfn 3.8 (dev) package was utilized to analyze ESP.

Through the calculation results of DFT, as shown in the figure, in the first conformation of the *E* configuration, the ESP of the fluoride ion will alternate with the ESP of the carbonyl O, both of which are negative values, mutually repelling each other, leading to a sharp increase in energy. In the second conformation of the *E* configuration, although there is no mutual repulsion between the ESP of the fluoride ion and the ESP of the substrate, the substrate molecule itself is relatively unstable, with a continuous large area of negative ESP. In the *Z* configuration, the first conformation is almost perfect, with the positive peak of the ESP of the substrate molecule perfectly alternating with the fluoride ion. In the second conformation, there is a certain alternation between the ESP of the fluoride ion and the ESP near the relatively positively charged S, causing an increase in energy. In the presence of the F^- ion, the potential peak point of the HTI-Indole molecule coincides highly with the F ion, proving the strong electrostatic interaction between the two. These explain why the addition of F^- ions can accelerate the HTI-Indole molecule's faster transition from the *E* configuration back to the Z configuration.

In addition, we also conducted DFT calculations on Cl ions, and the results are shown in Figure S17. The peak point of the Cl^- ion does not overlap with the ESP peak point because the interaction between the Cl^- ion and H is very weak, so there is a certain distance from the peak point of the substrate's ESP. This also explains why the energy is relatively higher compared to the F^- ion.

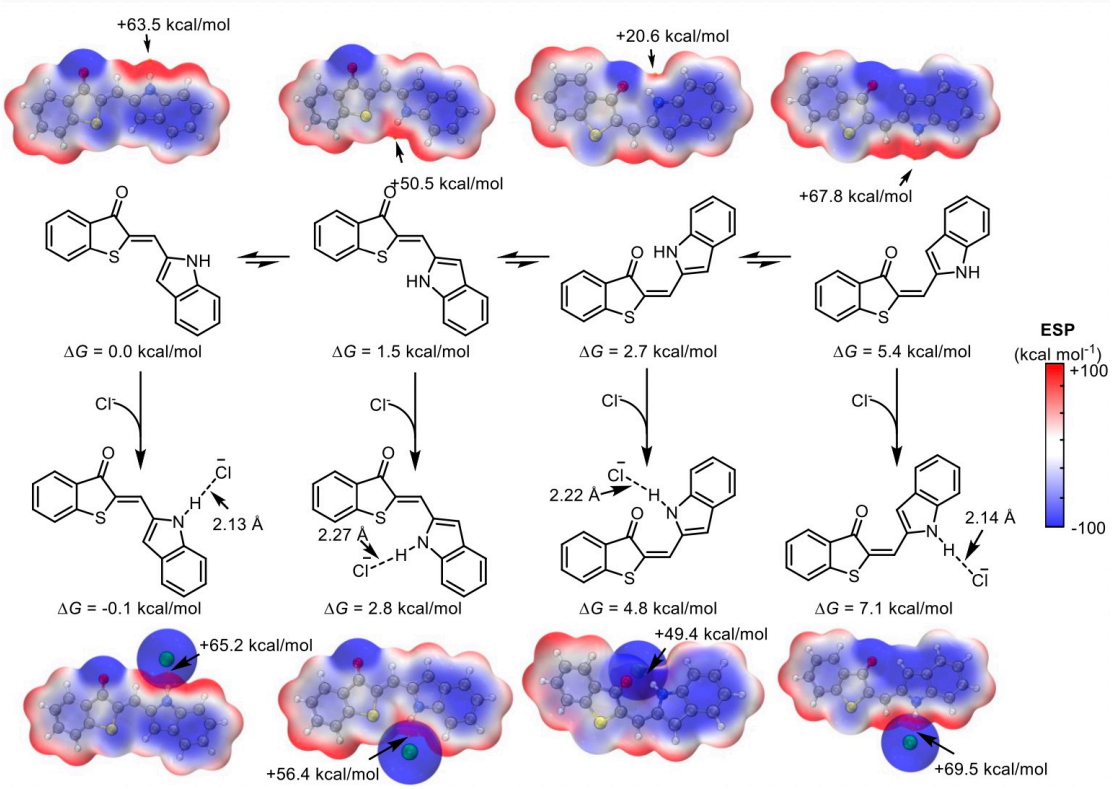

Fig. S17. Surface electrostatic potential maps of HTI-In molecule before and after the addition of chloride ions. All computational results were performed at the M06-2X/def2-TZVP/SMD//M06-2X/6-31G(d)/SMD level of theory. Geometrical optimization and single-point energies were obtained using the Gaussian 16C.01 package, while Multiwfn 3.8 (dev) package was utilized to analyze ESP.

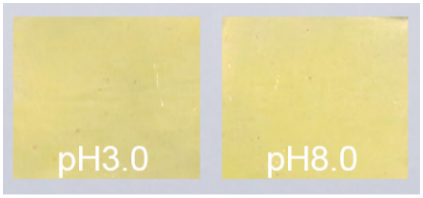

Fig. S18. Photographs of HTI-In-based pH sensor immersed in different pH aqueous solutions without 455 nm light.

5. Reference

1. S. Wiedbrauk, B. Maerz, E. Samoylova, A. Reiner, F. Trommer, P. Mayer, W. Zinth and H. Dube, *J. Am. Chem. Soc.*, 2016, **138**, 12219-12227.
2. C. Wurth, M. Grabolle, J. Pauli, M. Spieles and U. Resch-Genger, *Anal. Chem.,* 2011, **83**, 3431-3439.